# Optimizing the Electrical Stimulation of Retinal Ganglion Cells

A. E. Hadjinicolaou, C. O. Savage, N. V. Apollo, D. J. Garrett, S. L. Cloherty, M. R. Ibbotson, and B. J. O'Brien

***Abstract*—Epiretinal prostheses aim to restore visual perception in the blind through electrical stimulation of surviving retinal ganglion cells (RGCs). While the effects of several waveform parameters (e.g., phase duration) on stimulation efficacy have been described, their relative influence remains unclear. Further, morphological differences between RGC classes represent a key source of variability that has not been accounted for in previous studies. Here we investigate the effect of electrical stimulus waveform parameters on activation of an anatomically homogenous RGC population and describe a technique for identifying optimal stimulus parameters to minimize the required stimulus charge. Responses of rat A2-type RGCs to a broad array of biphasic stimulation parameters, delivered via an epiretinal stimulating electrode (200 $\times$ 200 $\mu$m) were recorded using whole-cell current clamp techniques. The data demonstrate that for rectangular charge-balanced stimuli, phase duration and polarity have the largest effect on threshold current amplitude—cells were most responsive to cathodic-first pulses of short phase duration. Waveform asymmetry and increases in interphase interval further reduced thresholds. Using optimal waveform parameters, we observed a drop in stimulus efficacy with increasing stimulation frequency. This was more pronounced for large cells. Our results demonstrate that careful choice of electrical waveform parameters can significantly improve the efficacy of electrical stimulation and the efficacy of implantable neurostimulators for the retina.**

***Index Terms*—Electrophysiology, epiretinal stimulation, patch clamp, rat, retinal prosthesis.**

Manuscript received February 16, 2014; revised July 08, 2014, August 15, 2014; accepted September 24, 2014. Date of publication October 17, 2014; date of current version March 05, 2015. This work was supported by the Australian Research Council through Discovery ProjectGrant DP0881247, by the Centre of Excellence in Vision Science under Grant CE0561903 by the Special Research Initiative in Bionic Vision Science and Technology (Bionic Vision Australia: SR1000005), and by the National Health and Medical Research Council of Australia Project Grant GNT0585440.

A. E. Hadjinicolaou, S. L. Cloherty, and M. R. Ibbotson are with the National Vision Research Institute, Australian College of Optometry, VIC, Australia, and the Centre of Excellence for Integrative Brain Function and Department of Optometry and Vision Sciences, University of Melbourne, VIC, Australia.

C. O. Savage was with the NeuroEngineering Laboratory, Department of Electrical and Electronic Engineering, University of Melbourne, VIC, Australia; and the Centre for Neural Engineering, University of Melbourne, VIC, Australia.

N. V. Apollo is with the School of Physics, University of Melbourne, VIC, Australia.

D. J. Garrett is with the School of Physics, University of Melbourne, VIC, Australia, and the Bionics Institute, East Melbourne, VIC, Australia.

B. J. O'Brien was with the National Vision Research Institute, Australian College of Optometry, VIC, Australia, and the Centre of Excellence for Integrative Brain Function and Department of Optometry and Vision Sciences, University of Melbourne, VIC, Australia.

Digital Object Identifier 10.1109/TNSRE.2014.2361900

## I. Introduction

RETINAL prostheses aim to restore visual perception to patients suffering vision loss caused by degenerative diseases of the retina. These devices employ electrical stimulation of the retina in an attempt to replicate the afferent neural signal normally conveyed from the retina to the brain to affect vision. The primary neural target for epiretinal electrical stimulation in the degenerate retina is the surviving population of retinal ganglion cells (RGCs), which forms a set of parallel pathways into the visual system. Each morphological RGC type conveys a specific type of visual information to specific targets in the brain [1].

While clinical trials to date have achieved considerable success, the vision conveyed to implant recipients has been rudimentary at best (for review, see [2]). Realizing the full potential of retinal implants is critically dependent on improving our understanding of the neural response of the retina to electrical stimulation. To this end, a number of studies have investigated the effect of different waveform parameters on the efficacy of RGC activation. Broadly, cathodic current pulses are reported to result in lower absolute thresholds when stimulating in the epiretinal space [3], [4], short duration pulses are reported to activate RGCs directly while longer pulses cause additional activation of presynaptic neurons [4]–[6] and thresholds for repetitive stimulation are reported to increase as pulse rate increases, although the precise relationship is seemingly dependent on cell type [7], [8].

Despite this emerging picture, to date there has been no systematic study of the relative impact of different waveform parameters on RGC activation and no attempt to objectively identify optimal stimulus waveform parameters for a specific morphological RGC class. Notably, prior studies have often comprised relatively few cells of any given type and have typically explored the effect of only one stimulus parameter in isolation. Further, in most prior studies recorded cells are classified based on functional signatures of their response to light stimuli (e.g., ON or OFF, transient or sustained responses). These groupings are likely comprised of multiple RGC types and are therefore confounded by variability that could plausibly be attributed to intrinsic differences among different morphological RGC types [9]–[12].

In this study we employ whole-cell patch clamp recordings from morphologically identified A2-type retinal ganglion cells in the rat retina to explore the effect of stimulation waveform parameters (polarity, phase duration, interphase interval and asymmetry) on the efficacy of epiretinal electrical stimulation. We first quantify the relative sensitivity of stimulus efficacy to the different waveform parameters. We then demonstrate a strategy

for identifying optimal stimulation parameters, minimizing the injected charge for a target stimulus efficacy. This constitutes the first reported attempt to objectively identify optimal stimulus waveform parameters for a single target RGC type. Using optimal stimulus parameters we then explore the effect of frequency on the efficacy of repetitive stimulation. Notably, we observe differential effects even within a single morphological cell type.

## II. Methods

All experimental procedures were performed according to the policies of the National Health and Medical Research Council of Australia and were approved by the Animal Experimentation Ethics Committee of the Faculty of Science at the University of Melbourne (approval 1112196).

### A. Retinal Wholemount Preparation

Data came from 26 pigmented Sprague-Dawley rats ranging in age from 3–5 months. Animals were anaesthetized with a mixture of Ketamine (100 mg $kg^{-1}$) and Xylazine (10 mg $kg^{-1}$) and enucleated. Rats were sacrificed with an overdose of Sodium Pentobarbitone (350 mg, intracardiac) after enucleation. Retinal wholemounts were placed ganglion cell layer up in the recording chamber and held in place with a stainless steel harp fitted with Lycra threads (Warner Instruments, CT USA). Once mounted in the chamber, the retina was perfused (4–6 ml $min^{-1}$) with carbogenated Ames' medium (Sigma-Aldrich, St. Louis, MO) and heated to 34 °C. The chamber was mounted on the stage of an upright microscope (BX51WI, Olympus) fitted with a 40× water-immersion lens. The microscope was fitted with a CCD camera (Ikegami, ICD-48E), which was used to visualize the retinal tissue on a monitor with 4× additional magnification.

### B. Physiological Data Collection

To obtain a whole-cell recording, a small opening was first made in the inner limiting membrane and optic fiber layer covering a ganglion cell [9], [13], [14]. Large-diameter RGCs with smooth surfaces and agranular cytoplasm exposed during this procedure were targeted for recordings. The pipette internal solution contained (in mM): K-gluconate 115, KCl 5, EGTA 5, HEPES 10, Na-ATP 2, Na-GTP 0.25; (mOsm = 273, pH = 7.3) including Alexa Hydrazide 488 (250 $\mu$M) and biocytin (0.5%). Whole-cell current-clamp recordings were obtained according to standard procedures [15], and the pipette series resistance was measured and compensated for using bridge balance circuitry. Initial pipette resistance ranged from 3–7 MΩ. Prior to recording, the pipette-offset voltage in the bath was nulled. After obtaining a gigaohm seal and rupturing the cellular membrane, the pipette series resistance was measured again to confirm break-in. Resting potentials were corrected for the change in liquid junction potential [16] that occurs upon break-in and cell dialysis. The liquid junction potential was measured directly as −11 mV. Capacitance compensation was not employed.

Membrane potential was amplified (BA-1S, NPI), digitized with 16-bit precision at 50 kHz (USB-6221, National Instruments) and stored in digital form. Collected data were analyzed off-line with custom software developed in MATLAB (MathWorks). Extracellular stimuli were generated by an external constant current source (MCS-4004, Multi-Channel Systems) and delivered through a single 200 × 200 $\mu$m square nitrogen-doped diamond electrode (described in [17]) placed upon the inner limiting membrane of the retina immediately adjacent to the recorded cell. Contact with the inner limiting membrane was evident when surface deformation of the retina could be seen under the microscope. Stimulating electrode resistances varied between 4–6 kΩ. A silver chloride-coated silver ball electrode situated approximately 5 mm from the cell provided an electrical return.

### C. Electrode Fabrication

Thin films (50 $\mu$m) of nitrogen doped ultra-nanocrystaline diamond (N-UNCD) were grown in an Iplas microwave plasma assisted chemical vapor deposition (CVD) system. Samples were grown with a gas mixture of $20:79:1$ $N_2:Ar:CH_4$ under conditions previously described [18]. The 200 × 200 $\mu$m square electrodes were glued to stainless steel shafts with conducting silver epoxy (Circuit Works). The assembly was cleaned by sequential ultrasonication in acetone (10 min), isopropyl alcohol (1 min), and deionized water (1 min). Finally, the metal shaft and the back and sides of the diamond electrode were insulated by hand application of epoxy resin (Araldite). Electrical connection between the electrode and the stimulator was made by way of the stainless steel shaft. The electrodes were electrochemically activated using the procedure outlined by [18].

### D. Immunocytochemistry and Morphological Identification

Following recordings, the retinal tissue was removed from the chamber, mounted onto filter paper, fixed for 45 minutes in phosphate-buffered 4% paraformaldehyde, and stored in the dark for up to 2 weeks in 0.1 M phosphate-buffered saline (PBS; pH 7.4) at 4 °C. The tissue was subsequently processed on Superfrost plus slides to reveal biocytin-filled cells by incubation in 0.5% Triton X-100, 20 mg $mL^{-1}$ streptavidin conjugated to Alexa 488 (Invitrogen) in PBS overnight at room temperature. Tissue was thoroughly washed in PBS and stained with propidium iodide for roughly 8 minutes revealing the boundaries of the inner plexiform layer (IPL) by staining the nuclei of cells in the inner nuclear (INL) and ganglion cell layers (GCL). After additional washes in PBS, samples were protected in 60% glycerol using a coverslip. Filled cells were scanned by confocal microscopy (Zeiss PASCAL) and their morphology reconstructed in 3D (Fig. 1). Cells were classified according to previously established morphological parameters for rat RGCs [11], [19]–[21].

### E. Experimental Protocol

The primary aim of this study was to characterize the most effective electrical waveform for extracellular activation of RGCs. Stimulus waveforms were limited to trains of rectangular current pulses, as employed by current-generation retinal prostheses [2]. All stimuli employed here were biphasic and charge-balanced so as to prevent the production of toxic chemical species and maintain electrode integrity [22]. Such waveforms can be fully described by five parameters—phase

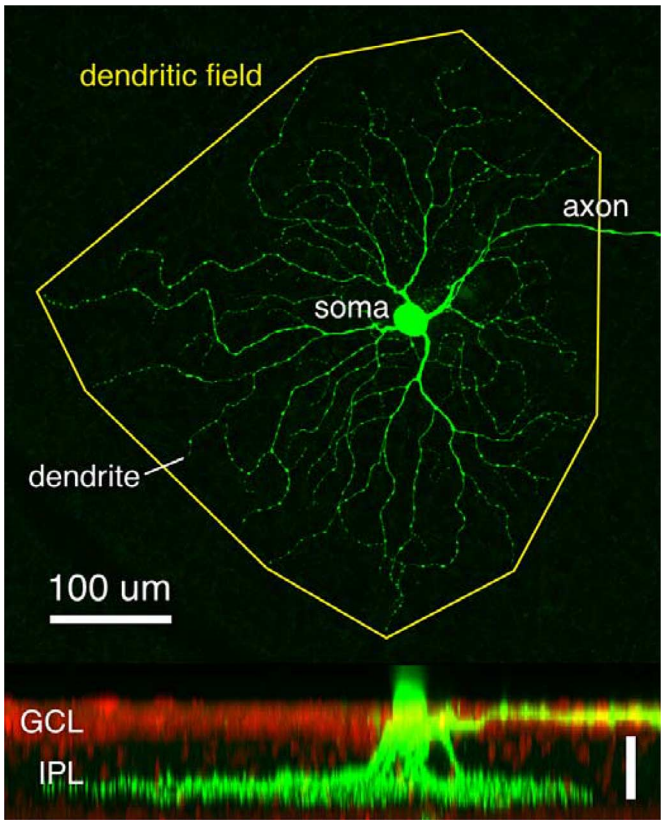


Fig. 1. Confocal reconstruction of an A2 (outer) retinal ganglion cell, with en face (top) and lateral (bottom) views. The cell was filled with biocytin and labelled with streptavidin-Alexa 488 (green). Cells in the ganglion cell layer (GCL) and inner nuclear layer were labelled with propidium iodide (red) to reveal the laminar extent of the inner plexiform layer (IPL). The yellow lines reveal the polygon used to determine the dendritic field area. Vertical scale bar: 20 $\mu$m.

duration ($\mathrm{pd}_1$ and $\mathrm{pd}_2$), asymmetry (defined by phase duration ratio $\mathrm{PDR} = \mathrm{pd}_2/\mathrm{pd}_1$), interphase interval (ipi), polarity (negative-leading biphasic pulses are referred to as cathodic-first), and frequency [Fig. 2(A) and (B)].

Prior to performing the experiment, each cell was subjected to brief depolarizing currents delivered by way of the recording pipette to ensure viability of the cell and stability of the recording. Viable cells, which produced a robust response to intracellular current injection (consistency and positive spike overshoot), were then subjected to further investigation using extracellular stimulation. A supra-threshold biphasic current pulse delivered through the stimulating electrode almost always evoked a single spike [Fig. 2(C)], although for a small number of cells, bursts of two or three spikes were observed on occasion. Efficacy was defined as the percentage of delivered biphasic stimuli that evoked at least one spike. Prior to pursuing an optimized stimulus waveform, we first surveyed the available parameter space using a fractional factorial design [23] to address the question of which waveform parameters have the greatest effect on charge threshold, the output metric of this survey. Stimulus efficacy of a given stimulus amplitude (or charge) was computed online during the experiment. Typically, this was done by starting with a small current amplitude and successively increasing amplitude over subsequent trials until the stimulus evoked an action potential on approximately 50%

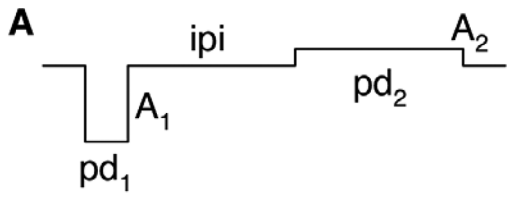


B

| n | $\mathrm{pd}_1$ | $\mathrm{pd}_2$ | ipi | pol |
|---|---|---|---|---|
| 1 | 200 | 400 | 240 | – |
| 2 | 200 | 400 | 240 | + |
| 3 | 60 | 180 | 420 | – |
| 4 | 200 | 600 | 600 | + |
| 5 | 480 | 480 | 420 | – |
| 6 | 480 | 1920 | 60 | + |
| 7 | 480 | 1440 | 60 | – |
| 8 | 340 | 340 | 420 | + |
| 9 | 60 | 240 | 240 | – |
| 10 | 340 | 1360 | 600 | + |
| 11 | 340 | 680 | 600 | – |
| 12 | 60 | 60 | 60 | + |

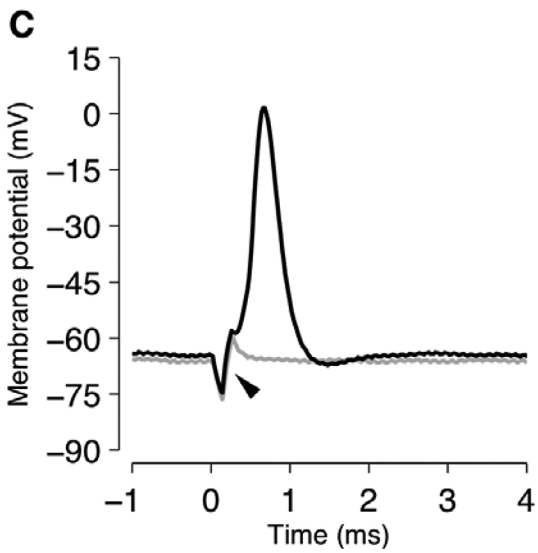


Fig. 2. (A) Schematic of a rectangular, biphasic waveform, demonstrating the parameters ($\mathrm{pd}_{1,2}$, first and second phase durations; $\mathrm{pd}_2/\mathrm{pd}_1 = \mathrm{PDR}$, phase duration ratio; ipi, interphase interval; and frequency) under consideration in this study. All waveforms are charge balanced such that $\mathrm{pd}_1 \times \mathrm{A}_1 = \mathrm{pd}_2 \times \mathrm{A}_2$. (B) Set of waveform parameters used in the preliminary investigation. Phase durations and interphase interval are in units of microseconds. Cathodic-first pulses are indicated with a minus symbol, anodic-first with a plus symbol. (C) Raw RGC membrane potential traces of two responses to a cathodic-first, symmetric, biphasic pulse with 120 $\mu$s phase duration, with stimulus onset at time t = 0 ms. Gray trace shows an isolated stimulus artifact (indicated by the arrowhead) and features no biological response. Black trace shows the stimulus artifact and a subsequently evoked action potential.bar: 20 $\mu$m.

of the pulses in the trains. Owing to the intrinsic variability of neural responses, finding the stimulus amplitude leading

to exactly 50% efficacy would have required an impractical number of trials (adjusting the stimulus amplitude by increasingly smaller amounts each time). We thus accepted efficacy in the range of 40%–50% to define the threshold stimulus current amplitude. The mean efficacy at "threshold" across all cells in our sample was 45%±5%.

The results from this preliminary investigation were used to inform the design of a baseline waveform, which served as the starting point for the subsequent waveform optimization protocol in which stimulus waveform parameters were optimized to maximize efficacy. In the final stage of the experiment, the frequency protocol, the optimized stimulus waveform was employed to investigate the effect of stimulus frequency. Stimulus waveform efficacy was the output metric of the waveform optimization and frequency protocols.

*1) Preliminary Investigation:* The charge balanced biphasic stimulus waveform is completely described by five parameters ($\mathrm{pd}_1, \mathrm{PDR} = \mathrm{pd}_2/\mathrm{pd}_1$, ipi, polarity and frequency). Charge thresholds were measured for both cathodic- and anodic-first stimuli with four levels of first-phase duration ($\mathrm{pd}_1 = 60$ $\mu$s, 200 $\mu$s, 340 $\mu$s, 480 $\mu$s), four levels of asymmetry ($\mathrm{PDR} = 1, 2, 3, 4$), and four levels of interphase interval (ipi $= 60$ $\mu$s, 240 $\mu$s, 420 $\mu$s, 600 $\mu$s). An exhaustive search of this parameter space for a given frequency would involve the testing of $4^3 \times 2 = 128$ different waveforms—a prohibitively large number for intracellular recordings. We therefore used a minimal set of 12 electrical waveforms [Fig. 2(B)] defined by a fractional factorial design (see [24] for a review of several biotechnological applications of this methodology) to quantify first-order parameter effects. Although this process greatly reduced the time commitment, the protocol still required up to 30 minutes for each recorded cell, which was achievable during recordings for 29 cells. The waveforms were presented in random order in the form of trains of ten biphasic current pulses delivered at a rate of 2 Hz. Each stimulus condition was delivered at threshold amplitude and repeated three times.

*2) Waveform Optimization Protocol:* Broad findings from the preliminary investigation were used to define a baseline waveform consisting of a symmetrical, cathodic-first pulse of short phase duration with no interphase interval. A phase duration of 120 $\mu$s was conservatively chosen to avoid using stimuli with excessively high current amplitudes (and the risk of exceeding the voltage compliance of the stimulating current source). In spite of this, we encountered a small number of cells (3 out of a total of 48 cells patched) for which threshold current amplitudes were sufficiently high that 40% efficacy could not be reached using phase durations of less than 100 $\mu$s. These cells were excluded from analysis. Beginning with this baseline waveform, the following procedure was then used to derive an optimized waveform:

1) Find threshold (40%–50% efficacy) for the baseline waveform.
2) Using threshold stimulus amplitude, test interphase intervals from 0–800 $\mu$s.
3) Update the baseline waveform with the most effective interphase interval between 0–100 $\mu$s.
4) Find threshold amplitude $\mathrm{I}_{\mathrm{th}}$ for the updated waveform ($\mathrm{pd}_1 = \mathrm{pd}_2 = 120$ $\mu$s).
5) Test all combinations of phase durations (60 $\mu$s, 120 $\mu$s, 240 $\mu$s, 480 $\mu$s) for both phases while preserving the charge per phase ($\mathrm{I}_{\mathrm{th}} \times 120$ $\mu$s) of the baseline waveform.
6) Update the waveform with the most effective phase durations.
7) Define this waveform as the optimized waveform.

During the waveform optimization protocol, stimuli consisted of trains of ten biphasic current pulses delivered at a rate of 2 Hz. Each stimulus condition was repeated at least three times.

*3) Frequency Protocol:* The optimized waveform, scaled to achieve at least 90% efficacy at 1 Hz was then used to investigate the effect of stimulus frequency. In the frequency protocol, stimuli consisted of pulse trains containing a maximum of 50 pulses, delivered at frequencies ranging from 1–200 Hz. Each stimulus frequency was repeated at least twice. For each stimulus frequency, efficacy was quantified as the percentage of stimulus pulses that evoked an action potential.

### *F. Data Analysis*

All data analysis was performed using custom software developed in MATLAB (MathWorks). Efficacy curves were generated by fitting a two-parameter logistic function to the data. In all cases, efficacy was defined as the proportion of stimulus events that evoked at least one action potential from the recorded cell.

When we varied stimulus frequency we also explored the effect of cell size. Two subsets of cells (large and small) were identified on the basis of either: 1) dendritic field size or 2) soma size. Cells with dendritic field diameters exceeding 460 $\mu$m were designated as large cells, while cells with dendritic field diameters less than 360 $\mu$m were designated as small cells. In terms of soma size, cells were defined as large if their soma diameters were 23 $\mu$m or greater, while soma diameters of 20 $\mu$m or less were classified as small. The relationship between soma diameter and dendritic field diameter was confirmed by computing Pearson's linear correlation coefficient ($\rho = 0.383, \mathrm{p} = 0.028$).

Each trial consisted of 50 pulses delivered at a given frequency. Efficacy was calculated over two analysis windows. At each stimulus frequency the duration of the analysis windows was such that each contained ten stimulus pulses. Thus, at 5 Hz, each window was 2 seconds in duration while at 50 Hz each window was 0.2 seconds in duration. The start of the first (or early) window was coincident with the onset of the stimulus pulse train. The start of the second (late) window was delayed, with respect to the first, by an interval equal to the window duration. In effect, the early window quantified efficacy over pulses 1–10 of the stimulus pulse train while the late window quantified efficacy over pulses 21–30.

Efficacy for large and small cells was compared within these windows at each stimulus frequency tested. The statistical significance of any observed difference in efficacy between large and small cells was determined with a random permutation test [25]. Specifically, efficacy within the two analysis windows was calculated for each cell. Cells were then randomly assigned to one of two groups with the size of the two groups being equal to the size of the original large and small cell groups (i.e., group

assignment was randomly permuted). Efficacy was then averaged across cells within each group and the difference calculated. This permutation of group assignments was performed a minimum of 10 000 times, resulting in a null distribution of the expected difference in mean efficacy assuming cell size had no effect. The observed difference in the unpermuted data (i.e., the difference in the mean efficacy averaged across the original subsets of large and small cells) was deemed significant if the proportion of samples in the null distribution that exceeded the observed difference was less than 5% (i.e., $p < 0.05$).

Multilinear regression (regress in MATLAB) was used to construct a model for charge thresholds using data from the initial parameter survey. All model coefficients were nonzero over a 95% confidence interval.

## III. Results

We recorded physiological responses selectively from A2-type RGCs (5 ON cells and 35 OFF cells), which were classified on the basis of their morphological reconstructions (e.g., Fig. 1). We found no significant difference in threshold current amplitude for our sample of ON and OFF cells ($p = 0.31$, two-sample t-test; also see [5], [26], [27]), and so combined and analyzed all cells as a single population.

### A. Preliminary Investigation

Charge thresholds associated with each stimulus waveform described in Fig. 2(B) were measured and averaged across 29 RGCs. We employed multilinear regression to identify those factors contributing to the lowest charge thresholds. The analysis identified three regressors ($pd_1$, PDR, polarity) as significant factors (i.e., coefficients for these factors were significantly different from zero, $p < 0.05$) in determining charge thresholds. Based on these three parameters, observed charge thresholds ($Q_{th}$) were well predicted by a surface given by

$$Q_{\rm th}(\mathrm{pd}_1, \mathrm{pd}_2, \mathrm{pol}) = 5.4 + 0.044 \cdot \mathrm{pd}_1 + 3.8 \cdot (\mathrm{pd}_2/\mathrm{pd}_1) + 5.1 \cdot \mathrm{pol} \quad (1)$$

where phase durations ($pd_1$ and $pd_2$) are in units of microseconds, charge thresholds are in units of nanocoulombs, and polarity (pol) is either $-1$ (cathodic-first) or $+1$ (anodic-first). Fig. 3(A) demonstrates the agreement between predicted and average observed charge threshold for each of the 12 waveforms tested ($r^2 = 0.822$).

We can better assess the relative efficacy of each waveform by normalizing charge thresholds such that for each cell the lowest threshold has a value of 0 and the highest a value of 1. Normalized charge thresholds for each stimulus waveform, averaged across all 29 cells, are displayed as a bar graph in Fig. 3(B). Cells were most responsive to waveforms 3 and 9, which were both cathodic-first, asymmetric, and had the shortest first-phase duration [60 $\mu$s, see Fig. 2(B)]. The two waveforms resulting in the highest charge thresholds (waveforms 6 and 10) were anodic-first, asymmetric, and had long first-phase durations (340 $\mu$s and 480 $\mu$s).

This parameter survey demonstrates that cathodic-first pulses of short first-phase duration are effective in evoking neural activity with minimal charge. However, the effects of asymmetry

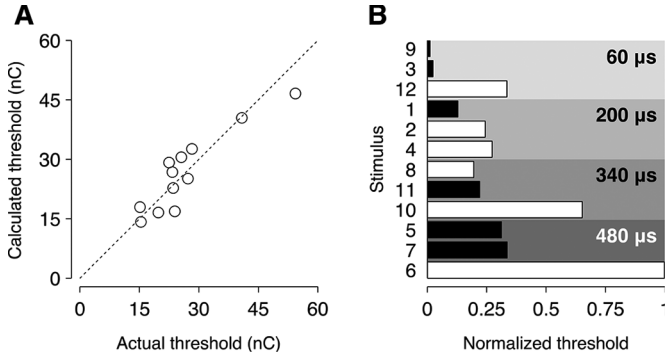


Fig. 3. Threshold current amplitude data from the preliminary investigation ($n = 29$). (A) Calculated versus actual charge thresholds. (B) Normalized charge thresholds averaged across all cells. White bars indicate anodic-first stimuli and black bars indicate cathodic-first stimuli. The data are ordered from top-to-bottom by increasing first-phase duration, which is listed for each group. The stimulus numbering scheme corresponds with that of Fig. 2(B).

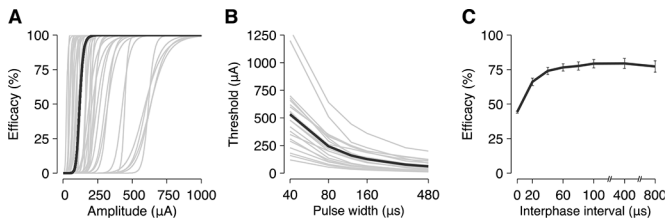


Fig. 4. (A) Efficacy curves ($n = 40$) fitted to experimental data. The median efficacy curve is indicated by the thick dark line. (B) Strength-duration curves ($n = 21$). The average strength-duration curve is indicated by the thick dark line. C: Efficacy as a function of interphase interval ($n = 40$). Error bars indicate plus/minus one standard error. Note that while addition of short interphase intervals ($<100$ $\mu$s) does increase efficacy, longer durations have little effect.

(responsible for both the highest and lowest charge thresholds) and interphase interval, which was not found to be a significant factor in the regression, remain unclear. Based on this result, we defined a baseline waveform as a symmetric, cathodic-first pulse of relatively short (120 $\mu$s) phase duration with no interphase interval. This baseline waveform provided a starting point for the waveform optimization protocol.

### B. Waveform Optimization Protocol

Using the baseline stimulus waveform described previously, we generated efficacy curves and estimated threshold stimulus amplitudes for 40 A2-type RGCs. Efficacy curves for each cell are plotted in Fig. 4(A). All fitted curves had an $r^2$ of $>0.9$, with the median value being 0.99. The median threshold stimulus amplitude was 164 $\mu$A. Strength-duration curves [Fig. 4(B)] were also generated for each cell by varying the phase duration (40–480 $\mu$s) of a symmetric cathodic-first biphasic pulse with no interphase interval. Threshold-versus-duration was well described by the Lapicque equation ($r^2 > 0.99$), as

$$I_{\rm th}(\mathrm{pd}) = I_r(1 + \tau/\mathrm{pd}) \quad (2)$$

where threshold current ($I_{th}$) is in units of microamps, phase duration (pd) is in units of microseconds, and with rheobase current $I_r = 4.5$ $\mu$A and chronaxie $\tau = 4.4$ ms.

*1) Interphase Interval:* To evaluate the impact of interphase interval on waveform efficacy, for each cell we first determined

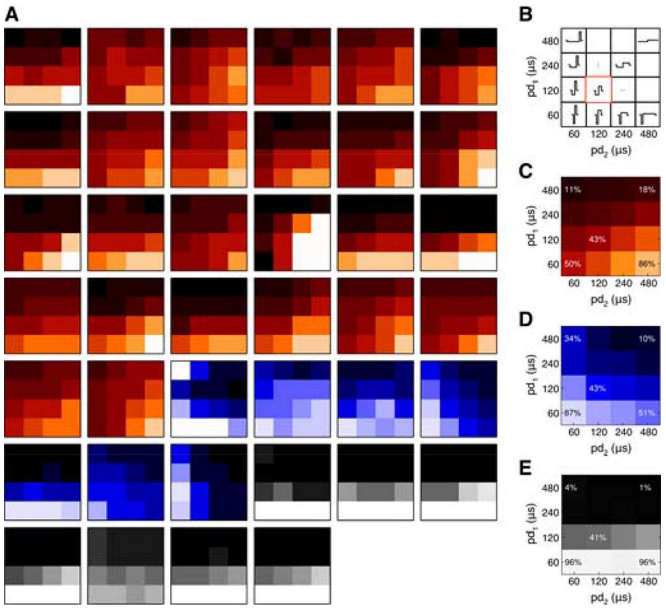


Fig. 5. (A) Efficacy as a function of phase duration for the waveform matrix ($n = 40$). Red: asymmetric waveform preference. Blue: symmetric waveform preference. Gray: short first-phase duration preference. Lighter shading indicates greater efficacy. An illustration of the waveforms in the matrix is seen in (B). Phase durations of 60 $\mu$s, 120 $\mu$s, 240 $\mu$s, and 480 $\mu$s were tested for both phases. Waveform highlighted by the red box indicates the baseline waveform at threshold amplitude. All waveforms maintain the per-phase charge of the baseline waveform. (C)–(E) Average efficacy as a function of phase duration for the waveform matrix, for each response category. Efficacy for selected waveforms is indicated as a percentage. Lighter shading indicates greater efficacy. Most cells preferred an asymmetric waveform (C) with $(\mathrm{pd}_1, \mathrm{pd}_2) = (60\ \mu\mathrm{s}, 480\ \mu\mathrm{s})$.

the threshold stimulus amplitude (at least 40% efficacy) for the baseline waveform, which had no interphase interval. We then added progressively longer interphase intervals and examined the consequent change in efficacy. The data show that efficacy was improved with the inclusion of an interphase interval [Fig. 4(C)]. At threshold amplitude, efficacy increased on average from 44% to 66% when increasing the interphase interval from zero to 20 $\mu$s. An additional increase to 40 $\mu$s increased efficacy to 74%. Introducing interphase intervals beyond 40 $\mu$s yielded only trivial improvements in efficacy. It is clear that the use of an interphase interval reduces threshold current amplitudes. However, improvement in efficacy saturates for interphase intervals greater than 100 $\mu$s.

*2) Asymmetry:* Prior to optimizing stimulus waveform asymmetry for each cell, the baseline waveform was updated to include the cells' optimal interphase interval. Threshold stimulus amplitude for each cell was then determined using this updated waveform. To identify optimal phase durations, we tested phase durations of 60 $\mu$s, 120 $\mu$s, 240 $\mu$s and 480 $\mu$s, while preserving the per-phase charge of the threshold stimulus amplitude. We present an illustration of the $4 \times 4$ waveform matrix evaluated using this protocol [Fig. 5(B)]. Fig. 5(A) shows efficacy matrices for 40 RGCs. Almost without exception, efficacy was greatest for waveforms with the shortest tested first-phase duration ($\mathrm{pd}_1 = 60\ \mu$s). We identified three general stimulus preferences among our sample of A2-type RGCs. The majority of cells (26/40 cells; 65%) preferred an asymmetric stimulus waveform

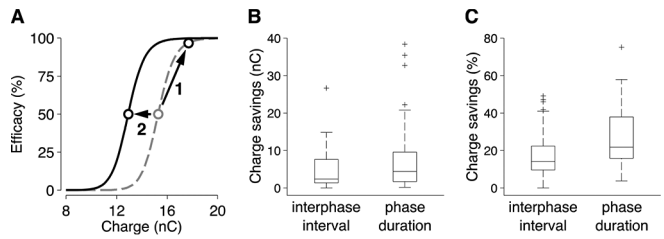


Fig. 6. (A) Charge savings for an example cell. Efficacy for the baseline stimulus waveform (dashed gray curve) can be improved by either increasing the injected per-phase charge (arrow 1) or by optimizing for interphase interval. The charge savings achieved after optimization effectively shift the efficacy curve to the left (arrow 2, solid black curve). (B), (C) Per-phase charge savings after waveform optimization ($n = 40$). (B) Raw charge savings. Median charge savings after optimizing interphase interval and phase duration were 2.1 nC and 4.2 nC, respectively. (C) Charge savings as a percentage of the pre-optimization charge. Median charge savings after optimizing interphase interval and phase duration were 14% and 20%, respectively.

($\mathrm{pd}_1 = 60\ \mu$s, $\mathrm{pd}_2 = 480\ \mu$s). For these cells, the observed efficacy of the asymmetric waveform was at least 10% greater than that of the symmetric waveform ($\mathrm{pd}_1 = \mathrm{pd}_2 = 60\ \mu$s). The efficacy matrices for these cells are shown in red [Fig. 5(A)]. A small proportion of cells (7/40 cells; 17.5%) preferred a symmetric stimulus waveform [blue efficacy matrices: Fig. 5(A)]. The remainder of our cell sample (7/40 cells; 17.5%) exhibited no clear preference for either symmetric or asymmetric stimulus waveforms [gray efficacy matrices: Fig. 5(A)]. For these cells, efficacy was determined almost entirely by the duration of the first phase, with a weak preference among some cells for asymmetric waveforms. To capture the mean efficacy signature for each of these three stimulus preferences (asymmetric, symmetric or indeterminate) we have averaged the cells within each group to create the matrices shown in Fig. 5(C)–(E).

*3) Relating Efficacy to Charge:* We can translate increases in efficacy to per-phase charge savings by using the efficacy curve generated in Fig. 4(A) to determine: 1) the threshold current before optimization, and 2) the amount of current required to achieve the same efficacy as the optimized waveform. The current difference is then converted to charge and expressed as a percentage of the per-phase charge before optimization [see Fig. 6(A)]. The efficacy curve for a single cell, generated using the baseline waveform parameters, is shown by the dashed gray curve. The predicted efficacy curve for this cell after optimizing the interphase interval (assuming the slope remains unchanged) is shown by the solid black curve. The threshold criterion (50% efficacy in this example) prior to waveform optimization defines the baseline-per-phase charge (15.3 nC). After waveform optimization, efficacy at this per-phase charge was increased from 50% to 97%. The amount of additional charge that would be required to generate an equivalent efficacy using the baseline waveform (2.4 nC, indicated by arrow 1) is then interpreted as charge saved. Waveform optimization effectively shifts the efficacy curve to the left (arrow 2). We present box-and-whisker plots of the charge savings as a result of optimizing interphase interval and phase duration for 40 RGCs [Fig. 6(B) and (C)]. Optimizing interphase interval led to a median charge saving of 14% and optimizing phase duration resulted in a median charge saving of 20%.

### C. Frequency Protocol

The optimized stimulus waveform for each cell, obtained after optimizing the interphase interval and phase duration of the baseline waveform, was used to test the effect of stimulus frequency on efficacy. Fig. 7(A) plots efficacy as a function of pulse number for stimulus frequencies ranging from 5–200 Hz. Efficacy decreases for consecutive stimulus pulses, converging to a frequency-dependent level after approximately 20 pulses. By the 20th pulse, efficacy for 20 Hz and 200 Hz had fallen to roughly 65% and 30% of efficacy at 1 Hz, respectively. Regardless of pulse number, increased stimulation frequency resulted in decreased efficacy [Fig. 7(A)]. In a subset of ten cells, we also investigated the effect of frequency on the stimulus current amplitude required to elicit at least 90% efficacy. For each cell, the stimulus current amplitude required to achieve at least 90% efficacy at each stimulus frequency was normalized to that required at a stimulus frequency of 1 Hz. We plot this normalized current amplitude, averaged across all cells tested $(\mathrm{n} = 10)$, at each of the stimulus frequencies tested [Fig. 7(B)]. This analysis shows that increased levels of current are required to sustain suprathreshold efficacy as frequency is increased and that this relationship is linear $(\mathrm{r}^2 > 0.99)$ and described by

$$I_{\mathrm{th}}(f) = 0.0027 \cdot f + 1.02. \tag{3}$$

The data show that A2 cell size impacts upon its ability to follow a train of electrical stimulus pulses. To quantify this, we partitioned our sample according to dendritic field (DF) size and compared the efficacy of different frequencies over two analysis windows: an early window and a late window. The early window quantified efficacy over the first ten stimulus pulses in a given stimulus train, while the late window quantified efficacy over pulses 21–30. Fig. 7(C) plots efficacy over the early analysis window as a function of stimulus frequency for cells with large (black) and small (gray) dendritic field sizes. Over the duration of the early analysis window [Fig. 7(C)], cells with smaller DFs are highly responsive to stimulation at all frequencies. Conversely, cells with large DFs exhibited a decrease in efficacy with increasing stimulus frequency. On average these cells managed to respond to only half of the stimulus pulses delivered at 100 Hz. This difference persisted over the duration of the late analysis window [Fig. 7(D)], where again small cells sustained activation at the highest stimulation frequencies tested. A similar analysis was performed after partitioning the cell population on the basis of soma diameter. Again, smaller cells were better able to sustain activation at high stimulus frequencies [Fig. 7(G), and (H)].

Histograms illustrating the distribution of dendritic field size ($416 \pm 53$ $\mu$m; mean $\pm$ std. dev.) and soma diameter ($22 \pm 2.5$ $\mu$m; mean $\pm$ std. dev.) are shown (Fig. 7(E) and (I), respectively) for the 37 RGCs tested (for three cells data for all frequencies could not be collected, so they were excluded from this analysis). Efficacy curves for large and small cells, based on dendritic field size and soma diameter, are shown in Fig. 7(F) and (J), respectively. The distributions of efficacy

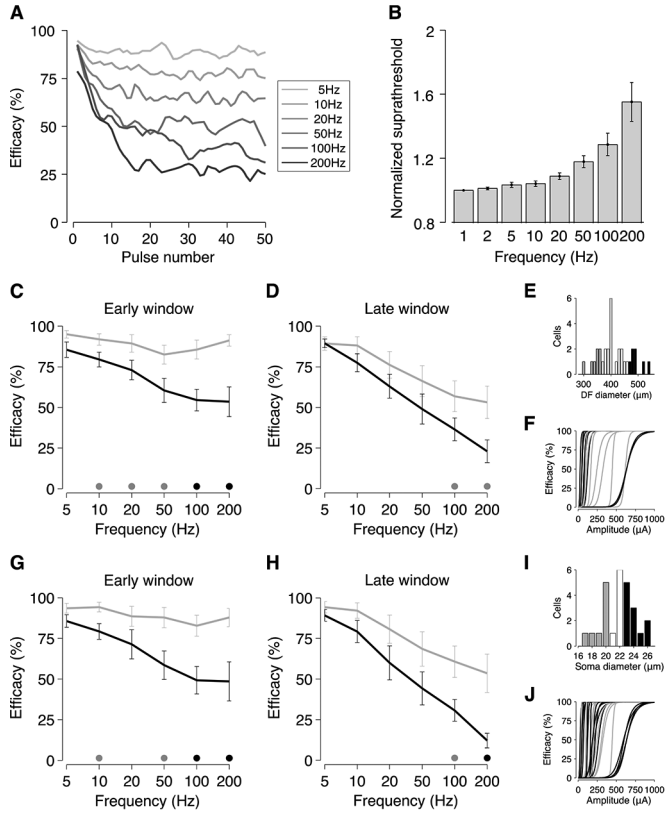


Fig. 7. Frequency dependence of stimulation. (A) Efficacy, plotted against consecutive pulse number, falls with frequency $(\mathrm{n} = 37)$. Curves were treated with a moving average (five points). (B) Normalized suprathreshold stimulus amplitude as a function of frequency $(\mathrm{n} = 10)$. Error bars indicate plus/minus one standard error. (C), (D) Differences in frequency response as related to dendritic field size. Small dendritic field diameters are defined as being $<360$ $\mu$m $(\mathrm{n} = 7)$, large dendritic field diameters $>460$ $\mu$m $(\mathrm{n} = 7)$. Error bars indicate plus/minus one standard error. Gray and black dots indicate statistically significant differences in the responses of the two cell populations ($\mathrm{p} < 0.05$ and $\mathrm{p} < 0.01$, respectively). Part (C) considers efficacy over the early analysis window (first ten stimuli pulses), while (D) considers pulses over the late analysis window (pulses 21–30). (E) Histogram of dendritic field diameter. Black: large somas, gray: small somas. (F) Efficacy curves [as in Fig. 4(A)], highlighting data from large dendritic field (black) and small dendritic field (gray) cells. (G), (H) Differences in frequency response as related to soma size. Small soma diameters are defined as being $\leq 20$ $\mu$m $(\mathrm{n} = 8)$, large soma diameters $\geq 23$ $\mu$m $(\mathrm{n} = 11)$. Error bars indicate plus/minus one standard error. Gray and black dots indicate statistically significant differences in the responses of the two cell populations ($\mathrm{p} < 0.05$ and $\mathrm{p} < 0.01$, respectively). Part (G) considers efficacy over the early analysis window (first ten stimuli pulses), while (H) considers pulses over the late analysis window (pulses 21–30). (I) Histogram of soma diameter. Black: large somas, gray: small somas. (J) Efficacy curves [as in Fig. 4(A)], highlighting data from large soma (black) and small soma (gray) cells.

curves for large (black) and small (gray) cells in each case suggest that thresholds are largely independent of cell size. Accordingly, we found no significant difference in threshold stimulus current amplitudes for large and small cells defined either according to dendritic field size (Wilcoxon rank sum test, $\mathrm{p} = 0.189$) or soma diameter $(\mathrm{p} = 0.937)$. While the relationship between cell size and threshold did not reach significance in our sample, the trend for large-field cells to have lower median thresholds (83 $\mu$A, compared with 247 $\mu$A) is in line with previous work [28], [29]. We observed no systematic relationship between optimal interphase interval or optimal phase durations and cell size.

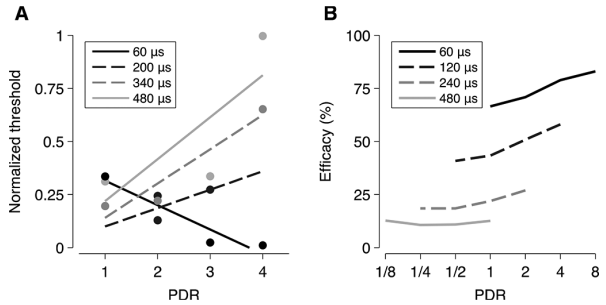


Fig. 8. (A) Normalized charge thresholds from the preliminary investigation and their relation to PDR and first-phase duration, regardless of other parameter values. The legend indicates first-phase duration. The gradients of the fitted lines suggest that asymmetry serves to reduce thresholds when the first phase is short enough ($\mathrm{pd}_1 = 60\ \mu$s). (B) Data from the waveform optimization protocol illustrate the relationship between efficacy and PDR, and how this varies with the duration of the first phase (indicated by the legend).

## IV. Discussion

This study sought to determine the waveform parameters of greatest influence on RGC threshold stimulus amplitudes and then characterise the most efficacious charge-balanced biphasic current waveform. We restricted our attention to a single morphological RGC type: the rat A2-RGC. The main findings were as follows: 1) threshold stimulus amplitudes are most sensitive to waveform polarity and phase duration; 2) the effect of asymmetry depends on phase duration; and 3) cell size is correlated with the ability to sustain repetitive stimulation at high frequency, even within cells of a single morphological class. The electrodes used were constructed from nitrogen-doped ultrananocrystaline diamond [18]. Previous tests have shown that electrodes made from this material behave in a similar fashion to electrodes made from more conventional stimulating materials [17]. Therefore, our results likely have broader relevance to other types of stimulating electrodes.

*1) Waveform Parameters:* We found cathodic-first biphasic current pulses to be more effective than anodic-first pulses for evoking spiking responses in A2-cells. This is consistent with predictions from computational modelling [30], [31] and with previous studies involving epiretinal electrical stimulation of retinal ganglion cells in other species (e.g., rat, guinea pig and monkey retinae: [32], rabbit retina: [33]). All evoked action potentials were initiated within a millisecond of stimulus onset, consistent with direct activation of the retinal ganglion cell [5].

Stimulus waveform asymmetry has been previously shown to reduce charge thresholds for electrical stimulation of cat and guinea pig auditory nerve fibers [34], [35]. However, asymmetry was reported to be inconsequential during electrical stimulation of rat auditory cortex [36]. In the present *in vitro* study of the rat retina, we found that the effect of asymmetry largely depends on the duration of the first phase. The regression model fitted to our data (1) predicts that charge thresholds increase with asymmetry and yet the two most effective waveforms are asymmetric [Fig. 3(B)]. To reconcile this, Fig. 8 shows normalized charge threshold plotted against phase duration ratio for each first-phase duration. For phase durations $>200\ \mu$s, waveform asymmetry results in higher normalized charge thresholds. Fig. 8(A), however, suggests that asymmetry serves to reduce charge thresholds if the first-phase duration is small enough [$\mathrm{pd}_1 = 60\ \mu$s, solid black line in Fig. 8(A)]. Results from the phase duration optimization experiments (Fig. 5) are summarized in Fig. 8(B) and support the assertion that asymmetry reduces charge thresholds (and, conversely, increases stimulus efficacy) over the range of phase durations considered (60–480 $\mu$s). The shortest first-phase duration always gave rise to the smallest charge thresholds [i.e., highest efficacy; solid black line in Fig. 8(B)]. Moreover, for the majority of cells, stimulus efficacy was further increased (i.e., threshold reduced) with increasing waveform asymmetry. These data demonstrate that the interactions between parameters also play a significant role in determining waveform efficacy.

We also found that stimulus efficacy improves with greater temporal separation between each phase. Increasing the interphase interval from 0 to 20 $\mu$s offers the largest gain in efficacy [from 44% to 66%; Fig. 4(C)], with successive increases in interphase interval resulting in smaller gains. Increasing interphase interval beyond 100 $\mu$s offers negligible improvement in efficacy. Our observation that a moderate interphase interval improves stimulus efficacy is congruent with previous reports of electrical stimulation thresholds for RGCs (tiger salamander: [37]) and auditory nerve fibers (cat: [34]; guinea pig: [38]).

*2) Implications for Retinal Prostheses:* The notion of "optimal" in this study relates to a waveform that evokes a certain level of neural activity using minimal charge. We found the optimal waveform to be a charge-balanced cathodic-first, asymmetric biphasic pulse of short phase duration with a short interphase interval. What kind of prosthetic vision might be afforded an implant wearer by such a stimulus waveform? Several groups have reported that responses to extracellular electrical stimulation of the retina consist of two components: a transient, short-latency response, attributed to direct RGC activation, and a slower longer-latency response, attributed to indirect RGC activation by way of the retinal network (isolated rabbit retina: [5], [6], [27]; isolated rat retina: [4]; *in vivo* cat cortex: [39]). Further, short-latency responses attributed to direct activation are reported to be preferentially evoked by stimuli of short duration while long-latency responses, attributed to indirect activation, are preferentially evoked by stimuli of longer duration [4], [6], [40]. Therefore, it seems likely that the optimal waveform we identified will preferentially activate RGCs directly. Indeed, the efficacy metric employed in our study, and which underlies our waveform optimization, reflects short-latency spiking responses of the recorded RGCs.

Although our epiretinal study of electrical RGC activation has found a cathodic-leading waveform to be most effective, it is likely that an alternative site of stimulation (e.g., subretinal electrode placement) will result in a different optimal waveform. Cathodic-first pulses are reported to be more effective than anodic-first pulses when the stimulating apparatus is positioned on the epiretinal surface, while the reverse is reported when stimuli are delivered in the subretinal space [4], [5], [32], [41].

Which approach ultimately yields better outcomes in the clinic remains to be seen and will likely depend on the site of intervention and the nature of degeneration in the patient. One advantage of subretinal and suprachoroidal implant placement is the potential for utilization of surviving retinal circuitry for visual processing—the electrical activation of bipolar and

horizontal cells over, or in addition to, retinal ganglion cells may lead to more localized phosphene generation [42], [43]. However, degenerative retinal diseases such as retinitis pigmentosa are characterized by extensive retinal reorganization in addition to widespread neuronal death [44]. It is likely that for severe degeneration, the function of surviving interneurons will be compromised. This assertion is supported by reports that synaptic responses from retinal interneurons are absent in late-stage degenerate mice [45]. It is conceivable that there is value in selectively achieving both direct and indirect activation of surviving RGCs. For example, it may be advantageous to target retinal interneurons in the early stages of disease and to target surviving retinal ganglion cells directly in later stages. By employing a suitable efficacy metric, e.g., one reflecting long-latency response components, the approach to stimulus waveform optimization demonstrated here could be used to identify optimized waveforms for achieving indirect activation of RGCs by way of retinal interneurons.

We found that stimulus efficacy fell with increasing stimulus frequency (Fig. 7). This is consistent with previous reports involving electrical stimulation of isolated rabbit retina [7], [8], [27], [46]. Fried *et al.* reported that short-duration ($<150$ $\mu$s per phase) pulses could be used to evoke reliably a single spike per pulse (i.e., direct RGC activation) at stimulation frequencies of up to 250 Hz [6]. However, higher stimulation frequencies necessitated greater stimulus amplitudes to reach threshold. The variability of this effect is considerable, not only across different functional cell types, but even within ganglion cells of a single functional class [8], [46]. Notably, this desensitization is observed in the absence of inhibitory amacrine cell input, which had previously been thought to play a key role in the suppression of the synaptic response [46]. Here we characterized the efficacy of repetitive stimulation for stimulus frequencies ranging from 1–200 Hz [Fig. 7(B)]. Over the range of frequencies considered, the relationship between threshold stimulus amplitude and stimulus frequency was linear.

There may be a connection between desensitization of RGC activation and the fading of visual percepts over time in human implant recipients [43], [47]. As suggested by Freeman and Fried, this fading may arise from the desensitization of a subset of RGCs, and not necessarily from desensitization of the entire ganglion cell population [46]. Consistent with this, they also reported a considerable amount of variability in the level of desensitization they observed, even among ganglion cells of a single functional class. Among the A2-RGCs we recorded, we found that small cells were better able to sustain repetitive activation when driven by trains of electrical stimuli at frequencies up to 200 Hz (Fig. 7). Our data suggest that variability in soma and dendritic field size has a substantial effect within cells of a single morphological type and that the subset of cells most susceptible to desensitization may be distinguished by size. Rat A2 (alpha) cell size has been demonstrated previously to increase with eccentricity [19] (but also see [20]). In our experimental recordings we did not control for eccentricity. It is possible that the effect of cell size we observed is confounded by other factors such as cell density, retinal thickness, or the thickness of the inner limiting membrane, all of which are well known to decrease with increasing eccentricity in mammalian retina. We have previously investigated the effect of the inner limiting membrane on electrical stimulation thresholds [48]. We found no substantive differences in threshold stimulus amplitude when stimulating electrodes were placed below, as opposed to above, the inner limiting membrane. Therefore, it seems unlikely that a systematic change in thickness of the inner limiting membrane could account for the effect that we observe.

## V. Conclusion

Our results show that, for epiretinal stimulation using rectangular biphasic current pulses, polarity and phase duration had the greatest effect on waveform efficacy, with further gains generally achieved by employing asymmetry and an interphase interval. We also discovered that within cells of a single morphological type (i.e., rat A2-type RGCs), smaller cells were better able to sustain repetitive activation at high frequency. The results of our investigation suggest that a careful choice of waveform parameters could significantly improve the efficacy of retinal prostheses.

## Acknowledgment

The Bionics Institute acknowledges the support they receive from the Victorian Government through its Operational Infrastructure Program.

## References

[1] D. M. Dacey, "Primate retina: Cell types, circuits and color opponency," *Prog. Retin. Eye Res.*, vol. 18, no. 6, pp. 737–763, Nov. 1999.
[2] J. D. Weiland, A. K. Cho, and M. S. Humayun, "Retinal prostheses: Current clinical results and future needs," *Ophthalmology*, vol. 118, no. 11, pp. 2227–2237, Nov. 2011.
[3] R. J. Jensen, J. F. Rizzo, O. R. Ziv, A. Grumet, and J. Wyatt, "Thresholds for activation of rabbit retinal ganglion cells with an ultrafine, extracellular microelectrode," *Invest. Ophthalmol. Vis. Sci.*, vol. 44, no. 8, pp. 3533–3543, Aug. 2003.
[4] D. Boinagrov, S. Pangratz-Fuehrer, G. Goetz, and D. Palanker, "Selectivity of direct and network-mediated stimulation of the retinal ganglion cells with epi-, sub- and intraretinal electrodes," *J. Neural Eng.*, vol. 11, no. 2, p. 026008, Apr. 2014.
[5] R. J. Jensen, O. R. Ziv, and J. F. Rizzo, "Responses of rabbit retinal ganglion cells to electrical stimulation with an epiretinal electrode," *J. Neural Eng.*, vol. 2, no. 1, pp. S16–21, Mar. 2005.
[6] S. I. Fried, H. S. Hsueh, and F. S. Werblin, "A method for generating precise temporal patterns of retinal spiking using prosthetic stimulation," *J. Neurophysiol.*, vol. 95, no. 2, pp. 970–978, Feb. 2006.
[7] R. J. Jensen and J. F. Rizzo, "Responses of ganglion cells to repetitive electrical stimulation of the retina," *J. Neural Eng.*, vol. 4, no. 1, pp. S1–6, Mar. 2007.
[8] C. Cai, Q. Ren, N. J. Desai, J. F. Rizzo, and S. I. Fried, "Response variability to high rates of electric stimulation in retinal ganglion cells," *J. Neurophysiol.*, vol. 106, no. 1, pp. 153–162, July 2011.
[9] B. J. O'Brien, T. Isayama, R. Richardson, and D. M. Berson, "Intrinsic physiological properties of cat retinal ganglion cells," vol. 538.3, pp. 787–802, 2002.
[10] J. Qu and K. L. Myhr, "The morphology and intrinsic excitability of developing mouse retinal ganglion cells," *PLoS One*, vol. 6, no. 7, p. e21777, Jan. 2011.
[11] R. C. S. Wong, S. L. Cloherty, M. R. Ibbotson, and B. J. O'Brien, "Intrinsic physiological properties of rat retinal ganglion cells with a comparative analysis," *J. Neurophysiol.*, vol. 108, no. 7, pp. 2008–2023, Oct. 2012.
[12] C. Hu, D. D. Hill, and K. Y. Wong, "Intrinsic physiological properties of the five types of mouse ganglion-cell photoreceptors," *J. Neurophysiol.*, vol. 109, no. 7, pp. 1876–1889, Apr. 2013.
[13] D. W. Robinson and L. M. Chalupa, "The intrinsic temporal properties of alpha and beta retinal ganglion cells are equivalent," *Curr. Biol.*, vol. 7, no. 6, pp. 366–374, Jun. 1997.
[14] W. R. Taylor and H. Wässle, "Receptive field properties of starburst cholinergic amacrine cells in the rabbit retina," *Eur. J. Neurosci.*, vol. 7, no. 11, pp. 2308–2321, Nov. 1995.

[15] O. P. Hamill, A. Marty, E. Neher, B. Sakmann, and F. J. Sigworth, "Improved patch-clamp techniques for high-resolution current recording from cells and cell-free membrane patches," *Pflugers Arch.*, vol. 391, no. 2, pp. 85–100, Aug. 1981.
[16] bE. Neher, "Correction for liquid junction potentials in patch clamp experiments," *Methods Enzymol.*, vol. 207, no. 1991, pp. 123–131, Jan. 1992.
[17] A. E. Hadjinicolaou, R. T. Leung, D. J. Garrett, K. Ganesan, K. Fox, D. A. X. Nayagam, M. N. Shivdasani, H. Meffin, M. R. Ibbotson, S. Prawer, and B. J. O'Brien, "Electrical stimulation of retinal ganglion cells with diamond and the development of an all diamond retinal prosthesis," *Biomaterials*, vol. 33, no. 24, pp. 5812–5820, Aug. 2012.
[18] D. J. Garrett, K. Ganesan, A. Stacey, K. Fox, H. Meffin, and S. Prawer, "Ultra-nanocrystalline diamond electrodes: Optimization towards neural stimulation applications," *J. Neural Eng.*, vol. 9, no. 1, p. 016002, Feb. 2012.
[19] L. Peichl, "Alpha and delta ganglion cells in the rat retina," *J. Comp. Neurol.*, vol. 286, no. 1, pp. 120–139, Aug. 1989.
[20] K. R. Huxlin and A. K. Goodchild, "Retinal ganglion cells in the albino rat: Revised morphological classification," *J. Comp. Neurol.*, vol. 385, no. 2, pp. 309–323, Aug. 1997.
[21] W. Sun, N. Li, and S. He, "Large-scale morophological survey of rat retinal ganglion cells," *Vis. Neurosci.*, vol. 19, no. 4, pp. 483–493, 2002.
[22] D. R. Merrill, M. Bikson, and J. G. R. Jefferys, "Electrical stimulation of excitable tissue: Design of efficacious and safe protocols," *J. Neurosci. Methods*, vol. 141, no. 2, pp. 171–198, Feb. 2005.
[23] R. F. Gunst and R. L. Mason, "Fractional factorial design," *Wiley Interdiscip. Rev. Comput. Stat.*, vol. 1, no. 2, pp. 234–244, Sep. 2009.
[24] R. S. Rao, C. G. Kumar, R. S. Prakasham, and P. J. Hobbs, "The Taguchi methodology as a statistical tool for biotechnological applications: A critical appraisal," *Biotechnol. J.*, vol. 3, no. 4, pp. 510–523, Apr. 2008.
[25] B. Efron and R. J. Tibshirani*, An Introduction to the Bootstrap*. Boston, MA, USA: Springer US, 1993.
[26] C. Sekirnjak, P. Hottowy, A. Sher, W. Dabrowski, A. M. Litke, and E. J. Chichilnisky, "High-resolution electrical stimulation of primate retina for epiretinal implant design," *J. Neurosci.*, vol. 28, no. 17, pp. 4446–4456, Apr. 2008.
[27] D. Tsai, J. W. Morley, G. J. Suaning, and N. H. Lovell, "Direct activation and temporal response properties of rabbit retinal ganglion cells following subretinal stimulation," *J. Neurophysiol.*, vol. 102, no. 5, pp. 2982–2993, Nov. 2009.
[28] A. K. Cho, A. P. Sampath, and J. D. Weiland, "Physiological response of mouse retinal ganglion cells to electrical stimulation: Effect of soma size," in *Proc. IEEE Conf. Eng. Med. Biol. Soc.*, Jan. 2011, vol. 2011, pp. 1081–1084.
[29] S. I. Fried, A. C. W. Lasker, N. J. Desai, D. K. Eddington, and J. F. Rizzo, "Axonal sodium-channel bands shape the response to electric stimulation in retinal ganglion cells," *J. Neurophysiol.*, vol. 101, pp. 1972–1987, 2009.
[30] F. Rattay, "The basic mechanism for the electrical stimulation of the nervous system," vol. 89, no. 2, pp. 335–346, 1999.
[31] F. Rattay, L. P. Paredes, and R. N. Leao, "Strength-duration relationship for intra- versus extracellular stimulation with microelectrodes," *Neuroscience*, vol. 214, pp. 1–13, July 2012.
[32] C. Sekirnjak, P. Hottowy, A. Sher, W. Dabrowski, A. M. Litke, and E. J. Chichilnisky, "Electrical stimulation of mammalian retinal ganglion cells with multielectrode arrays," *J. Neurophysiol.*, vol. 95, no. 6, pp. 3311–3327, June 2006.
[33] M. Eickenscheidt, M. Jenkner, R. Thewes, P. Fromherz, and G. Zeck, "Electrical stimulation of retinal neurons in epiretinal and subretinal configuration using a multicapacitor array," *J. Neurophysiol.*, vol. 107, no. 10, pp. 2742–2755, May 2012.
[34] R. K. Shepherd and E. Javel, "Electrical stimulation of the auditory nerve: II. Effect of stimulus waveshape on single fibre response properties," *Hear. Res.*, vol. 130, no. 1–2, pp. 171–188, Apr. 1999.
[35] C. A. Miller, B. K. Robinson, J. T. Rubinstein, P. J. Abbas, and C. L. Runge-Samuelson, "Auditory nerve responses to monophasic and biphasic electric stimuli," *Hear. Res.*, vol. 151, no. 1–2, pp. 79–94, Jan. 2001.
[36] A. S. Koivuniemi and K. J. Otto, "Asymmetric versus symmetric pulses for cortical microstimulation," *IEEE Trans. Neural Syst. Rehabil. Eng.*, vol. 19, no. 5, pp. 468–476, Oct. 2011.
[37] A. C. Weitz, M. R. Behrend, M. S. Humayun, R. H. Chow, and J. D. Weiland, "Interphase gap decreases electrical stimulation threshold of retinal ganglion cells," in *Conf. Proc. IEEE Eng. Med. Biol. Soc.*, Jan. 2011, vol. 2011, pp. 6725–6728.
[38] P. Prado-Guitierrez, L. M. Fewster, J. M. Heasman, C. M. McKay, and R. K. Shepherd, "Effect of interphase gap and pulse duration on electrically evoked potentials is correlated with auditory nerve survival," *Hear. Res.*, vol. 215, no. 1-2, pp. 47–55, May 2006.
[39] S. D. Elfar, N. P. Cottaris, R. Iezzi, and G. W. Abrams, "A cortical (V1) neurophysiological recording model for assessing the efficacy of retinal visual prostheses," *J. Neurosci. Methods*, vol. 180, no. 2, pp. 195–207, Jun. 2009.
[40] E. Margalit and W. B. Thoreson, "Inner retinal mechanisms engaged by retinal electrical stimulation," *Invest. Ophthalmol. Vis. Sci.*, vol. 47, no. 6, pp. 2606–2612, Jun. 2006.
[41] A. Stett, A. Mai, and T. Herrmann, "Retinal charge sensitivity and spatial discrimination obtainable by subretinal implants: Key lessons learned from isolated chicken retina," *J. Neural Eng.*, vol. 4, no. 1, pp. S7–16, Mar. 2007.
[42] E. D. Cohen, "Prosthetic interfaces with the visual system: Biological issues," *J. Neural Eng.*, vol. 4, no. 2, pp. R14–31, Jun. 2007.
[43] E. Zrenner, K. U. Bartz-Schmidt, H. Benav, D. Besch, A. Bruckmann, V.-P. Gabel, F. Gekeler, U. Greppmaier, A. Harscher, S. Kibbel, J. Koch, A. Kusnyerik, T. Peters, K. Stingl, H. Sachs, A. Stett, P. Szurman, B. Wilhelm, and R. Wilke, "Subretinal electronic chips allow blind patients to read letters and combine them to words," in *Proc. Biol. Sci.*, May 2011, vol. 278, no. 1711, pp. 1489–1497.
[44] R. E. Marc, B. W. Jones, C. B. Watt, and E. Strettoi, "Neural remodeling in retinal degeneration," *Prog. Retin. Eye Res.*, vol. 22, no. 5, pp. 607–655, Sep. 2003.
[45] E. Margalit, N. Babai, J. Luo, and W. B. Thoreson, "Inner and outer retinal mechanisms engaged by epiretinal stimulation in normal and RD mice," pp. 145–154, 2011.
[46] D. K. Freeman and S. I. Fried, "Multiple components of ganglion cell desensitization in response to prosthetic stimulation," *J. Neural Eng.*, vol. 8, no. 1, p. 016008, Feb. 2011.
[47] A. P. Fornos, J. Sommerhalder, L. Cruz, J. A. Sahel, F. Hafezi, and M. Pelizzone, "Temporal properties of visual perception upon electrical stimulation of the retina temporal properties of visual perception upon electrical stimulation of the retina," vol. 41, no. 22, 2012.
[48] S. L. Cloherty, R. C. S. Wong, A. E. Hadjinicolaou, H. Meffin, M. R. Ibbotson, and B. J. O'Brien, "Epiretinal electrical stimulation and the inner limiting membrane in rat retina," in *Conf. Proc. IEEE Eng. Med. Biol. Soc.*, Jan. 2012, vol. 2012, pp. 2989–2992.

Authors' photographs and biographies not available at the time of publication.